GE), and Cy5 and Cy3 images were obtained by single scans. The Cy5 spot intensity was normalized with Cy3 for all protein spots by using the image analysis software Progenesis SameSpot (Non-linear Dynamics, Newcastle, UK). For preparative purposes, 100 μg of the protein sample was labeled with the Cy3 fluorescent dye and separated as described above. The protein spots of interest were matched between the images of analytical and preparative gels and recovered onto 96-well plates from the preparative gels by using our original spot-recovery machine (Molecular Hunter; AsOne, Osaka, Japan) [14]. The protein spots recovered were stored at 4 °C until use.

2.4. Statistical analysis

The protein expression profile data were exported as an XML file from the Progenesis SameSpot software and were imported to the data-mining software Expressionist (GeneData, Basel, Switzerland).

2.5. Mass spectrometric protein identification

The proteins were extracted as peptides from the protein spots by in-gel digestion as previously reported [14]. In brief, the protein spots recovered were washed extensively with acetonitrile and ammonium bicarbonate minimum solution and treated with trypsin (Promega, Madison, WI) at 37 °C overnight. Tryptic digests were recovered from the gel pieces, concentrated under vacuum, and resolubilized with 0.1% trifluoroacetic acid. The final tryptic digests were subjected to liquid chromatography with the Paradigm MS4 dual solvent delivery system (Michrom BioResources, Auburn, CA) and an LTQ linear ion trap MS (Thermo Electron, San Jose, CA) equipped with a nano-electrospray ion source (AMR, Tokyo, Japan). The Mascot software (version 2.3.02; Matrix Science Inc., Boston, MA) was used to search for the mass of the peptide ion peaks against the SWISS-PROT database (*Homo sapiens*, 471,472 sequences in the Sprot_57.5 fasta file). The MASCOT search parameters were as follows: the peptide tolerance was 1.3 Da, and the MS/MS tolerance was 1 Da (monoisotopic mass). Fixed modifications of carbamidomethylation and variable modifications of oxidation, 2+ and 3+ peptide charge were selected, and up to 3 missed trypsin cleavages were allowed. Proteins with a Mascot score of 34 or more were used for protein identification.

2.6. Western blotting

All the 45 protein samples used for 2D-DIGE were examined by western blotting. In brief, protein samples were separated by SDS-PAGE with Criterion TGX Precast Gels (Bio-Rad, Hercules, CA). Five micrograms of each protein was separated by SDS-PAGE, and the separated proteins were transferred to a nitrocellulose membrane. The protein transfer was achieved using a conventional western blotting buffer system. After blocking with skimmed milk for 1 h, the membrane was reacted with anti-CapG antibodies from Protreintech (Chicago, IL; 1:500 dilution) or GenWay (San Diego, CA; 1:1000 dilution) overnight. Subsequently, the membranes treated with the antibody from Proteintech or GenWay were treated with the second antibody against rabbit IgG (GE; 1:2000 dilution) or chicken IgY (Santa Cruz Biotechnology, Santa Cruz, CA; 1:4000), respectively. The membranes were processed by enhanced chemiluminescence (ECL Prime, GE). After the membranes were scanned with LAS-3000 (FujiFilm, Tokyo, Japan), they were stained with 0.2% Ponceau S and 1% acetic acid (Sigma Aldrich, St. Louis, MO), and the intensity of the protein bands was measured by the ImageQuant software (GE). The intensity of individual protein bands was normalized with the intensity of the lane on an identical membrane in the SDS-PAGE/western blots.

2.7. RNA interference, cell growth assay, and invasion assay

The human HLE cell line was obtained from the Health Science Research Resources Bank (Tokyo, Japan) and cultured in RPMI 1640 medium supplemented with 10% fetal bovine serum (Gibco BRL, Auckland, NZ). The target mRNA sequences for small interfering RNA (siRNA) were as follows for human CAPG: 5′-CAAGAGAACCAGGGCGUCUUCUUCU-3′ (siRNA 1) and 5′-GG CAAUGAGUCUGACCUCUUCAUGA-3′ (siRNA 2). A Stealth RNAi Negative Control Duplex (control siRNA), which was designed to minimize sequence homology to any known vertebrate transcript, was used as the control. The CAPG-specific (siRNA1 and siRNA2) and control siRNAs were purchased from Invitrogen (Carlsbad, CA). A total of 1×10^5 cells were seeded into each well of a 6-well tissue culture plate (Costar, Cambridge, MA). The cell monolayer was washed the next day with pre-warmed sterile phosphate-buffered saline (PBS). The cells were transfected with the siRNAs using Lipofectamine™ 2000 Reagent (Invitrogen) according to the manufacturer's protocol. Then, HLE cells were seeded at a density of 1.5×10^3 cells/well in 96-well plates. The cells were transfected the next day with the siRNAs, and after 3–5 days of culture, cell viability was measured using a cell counting kit (Dojindo Laboratories, Kumamoto, Japan) according to the manufacturer's instructions. After 2 h of incubation at 37 °C, the optical density was measured at a wavelength of 450 nm using a microplate reader. For protein extraction, the cells were washed twice with PBS, treated with 10% TCA for 30 min on ice, and scraped off into a tube. The cell pellet was incubated for 30 min in urea lysis buffer and centrifuged at 15,000 rpm for 30 min. The supernatant was recovered, and the protein concentration was measured with a protein assay kit (Bio-Rad, Hercules, CA). The samples recovered were subjected to western blotting to monitor the expression level of CaPG by using anti-CaPG antibody (Proteintech). Cell invasion was assayed in 24-well Biocoat Matrigel invasion chambers (8 μm; Becton Dickinson, Bedford, MA) according to the manufacturer's protocol. Briefly, the cells were treated with siRNAs, and on the following day, 1×10^4 cells were plated in the upper chamber. The bottom chamber contained 10% FBS as a chemoattractant. Forty-eight hours later, the noninvasive cells were removed with a cotton swab. The cells that migrated through the membrane and stuck to the lower surface of the membrane were fixed with methanol and stained with the Diff Quik stain (Sysmex, Hyogo, Japan). For quantification, the cells were photographed under a microscope at ×200 magnification and counted in 3 fields of triplicate membranes.

3. Results

3.1. 2D-DIGE with internal control samples

We created protein expression profiles using 2D-DIGE. Fig. 1A illustrates the design of the 2D-DIGE experiments. Cy5-labeled individual protein samples were mixed with a Cy3-labeled internal control sample and separated by 2D-PAGE. By normalizing the Cy5 intensity with the Cy3 control for all protein spots, the gel-to-gel variation could be compensated. This protocol enabled the examination of all 45 samples in this study by using 2 fluorescent dyes.

To observe larger numbers of protein spots, we used our original large-format 2D apparatus [14]. Fig. 1B shows a typical 2D image of the internal control sample. We assessed the

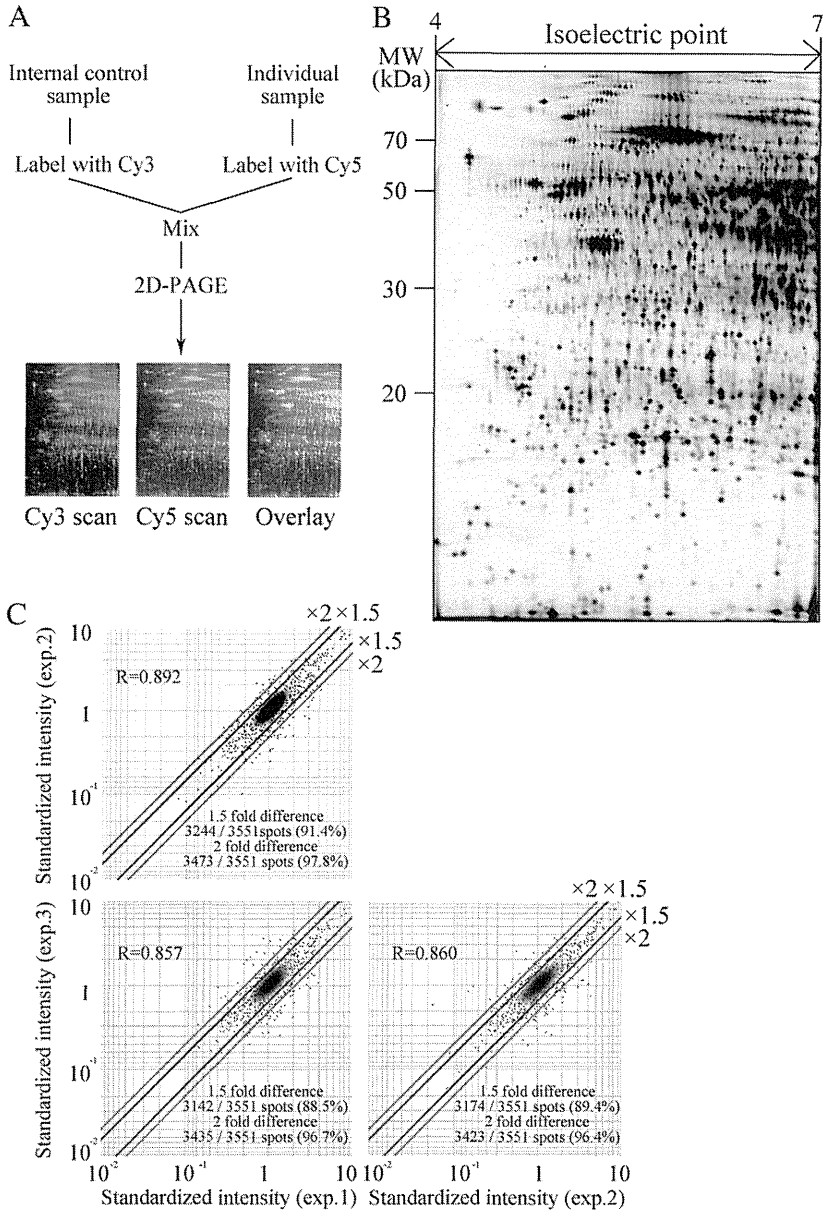

Fig. 1 – Overview of the 2D-DIGE experiments. A: Sample preparation for the 2D-DIGE experiments. The internal control and the individual samples were labeled with Cy3 and Cy5 fluorescent dyes, respectively. They were mixed together and separated by 2D-PAGE. After gel electrophoresis, the gel was scanned with a laser scanner. The spot intensity of the Cy5-labeled protein samples was normalized with the Cy3-labeled sample in the same gel. B: A typical 2D image of a Cy3-labeled internal control sample. The proteins were separated according to their isoelectric points and molecular weights. In total, 3491 protein spots were observed in a single gel. The enlarged 2D image is provided in Supplementary Figs. 1–3. C: Scattergrams show the system reproducibility. One sample was examined 3 times, and the intensities of individual protein spots were compared among the 3 experiments. Note that the correlation coefficient was at least 0.860, and the intensities of more than 88.5% of the protein spots had less than 1.5-fold differences.

system reproducibility of our proteomic study by examining the same sample 3 times. Fig. 1C shows the scattergrams for the triplicate experiments. The intensities of at least 88.5% of the scattered protein spots indicated less than 1.5-fold differences, and the relative coefficients were at least 0.857. The high reproducibility may be due to the use of the internal

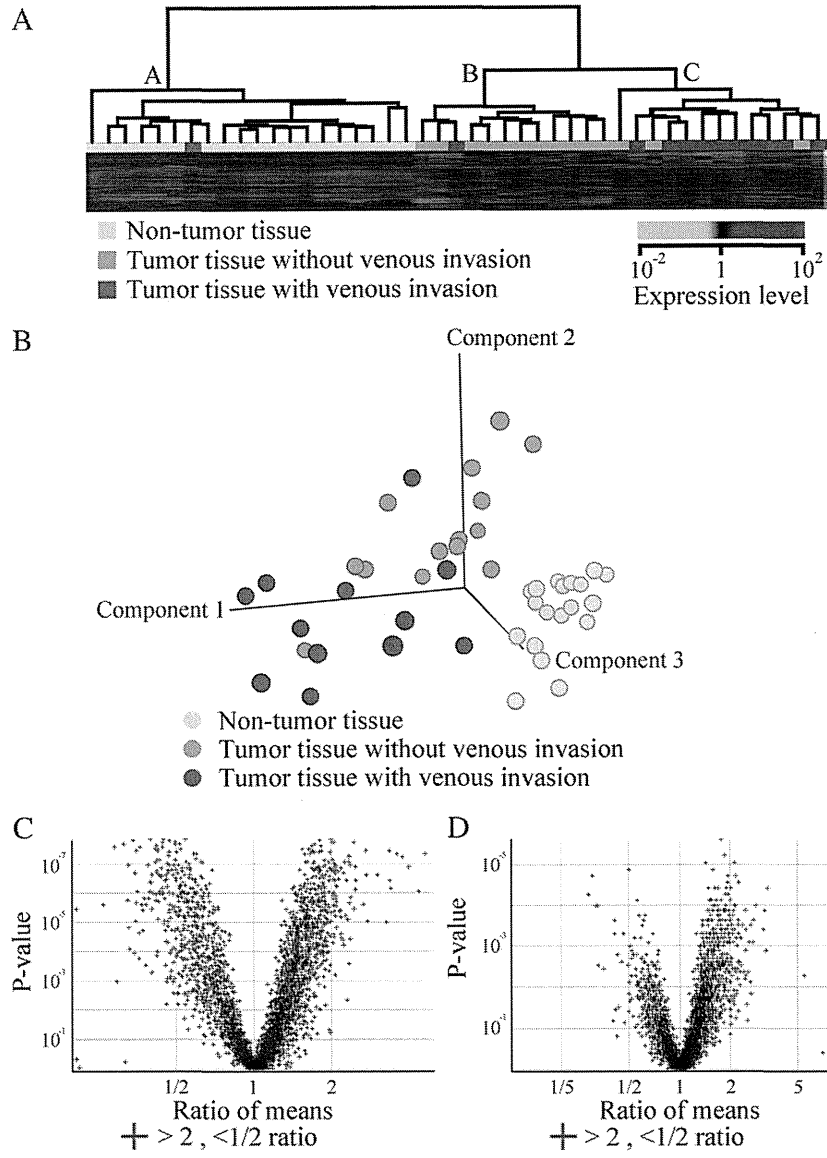

Fig. 2 – Overall features of the proteome examined by unsupervised classification. A: Samples were grouped by hierarchical clustering on the basis of the intensity of all 3491 protein spots. Note that the samples were mainly divided into 3 groups; most samples in tree A were non-tumor tissue samples, and the majority of samples in trees B and C were tumor tissue samples. The samples in trees B and C were tumor samples without and with vascular invasion, respectively. B: Samples were plotted in a three-dimensional space by principal component analysis based on the intensities of 3491 protein spots. Note that the samples were mainly divided into non-tumor tissues and tumor tissues. Tumor tissues were apparently divided into 2 groups, those with or those without vascular invasion. C: The 3491 protein spots were plotted as a function of fold differences and p-values, comparing non-tumor tissues with tumor tissues by a volcano plot. The ratio of means was calculated by dividing the averaged intensities of the tumor tissue samples with the non-tumor tissue samples. We identified 197 protein spots with statistically significant differences (fold difference>2; $p<0.05$) in intensity. D: The protein spots were plotted as a function of the fold differences and p-values on comparing the tumor tissues with and without portal vein invasion by using a volcano plot. The mean ratio was calculated by dividing the average intensity of the tumor tissue samples with vascular invasion with those with no vascular invasion. Note that 88 protein spots with statistically significant differences in intensity (fold difference>2; $p<0.05$) were identified. The spot intensities of all protein spots are summarized in Supplementary Table 2. The localization of the protein spots assessed by mass spectrometric protein analysis is shown in Supplementary Figs. 1–3.

control sample and the large format gels. We conducted the proteomic studies with this level of reproducibility.

3.2. Overall features of the proteome data generated by 2D-DIGE

First, we examined the overall features of the proteome by unsupervised classification. The protein samples were grouped by hierarchical clustering according to the intensity of 3491 protein spots (Fig. 2A). The normalized intensity of 3491 protein spots across 45 samples is summarized in Supplementary Table 2. The samples were divided into 3 major groups: trees A, B, and C. Tree A was mostly composed of the 19 non-tumor tissue samples, except for 1 tumor tissue sample. The majority of the samples in tree B were the 11 tumor tissues with no vascular invasion, except for 1 tumor tissue. Ten of the 13 samples in tree C were the tumor tissue samples with vascular invasion, and the rest were those without. Principal component analysis provided similar results (Fig. 2B). Overall, the non-tumor samples were discriminated from the tumor tissue samples, and the tumor tissues were separated according to the status of the vascular invasion.

We examined volcano plots to identify the proteins that were possibly responsible for the difference in the features between the tumor and non-tumor tissues and between the tumor tissues with vascular invasion and those without (Fig. 2C and D). The protein spots that exhibited a statistically significant difference (>2-fold difference; $p<0.05$) in intensity were selected for protein identification by mass spectrometry. In the comparison between the tumor and non-tumor tissue groups, we found that 197 protein spots met these criteria; 80 and 117 spots showed higher and lower intensities, respectively, in the tumor tissue group than in the non-tumor tissue (Fig. 2C). On comparing the tumor tissues with and without vascular invasion, we also found that there were 88 protein spots that met the abovementioned criteria; 72 and 16 spots had higher and lower intensities, respectively, in the tumor tissues with vascular invasion than in those without vascular invasion (Fig. 2D). The locations of these protein spots are shown in Supplementary Figs. 1 and 2.

We found that 23 protein spots were commonly identified in the following 2 sets of comparisons: the first being between non-tumor and tumor tissues and the second between tumor tissues with vascular invasion and those without. Among these 23 spots, 12 had a higher intensity in the tumor tissues than in the non-tumor tissues, and even higher intensities were observed in the tumor tissues with vascular invasion than in those without (Figs. 3 and 4). However, 6 protein spots had lower intensities in the tumor tissue group than in the non-tumor tissue group, and they showed lower expression in the vascular invasion-positive tumor tissues than in the vascular invasion-negative tumor tissues (Figs. 3 and 4).

3.3. Mass spectrometric protein identification of the protein spots with differing intensities between the sample groups

The 197 protein spots with differing intensities between the non-tumor tissues and tumor tissues were analyzed by mass spectrometry (Fig. 3). These 197 protein spots corresponded to 103 unique gene products. The list of identified proteins and the peptide data to support the protein identification are shown in Supplementary Tables 3 and 4, respectively. The locations of the 197 protein spots are shown in Supplementary Fig. 1. The 80 protein spots with higher intensities in the tumor tissue group corresponded to 54 unique gene products (Fig. 3A), and the 117 with lower intensities, to 64 unique gene products (Fig. 3B).

The 88 protein spots with differing intensities between the tumor tissues with vascular invasion and those without were also analyzed by mass spectrometry (Fig. 4). The list of the identified proteins and the peptide data to support the protein identification are shown in Supplementary Tables 5 and 6, respectively. The locations of the 88 protein spots are shown in Supplementary Fig. 2. The 88 protein spots corresponded to 55 unique gene products. The 72 protein spots with higher intensities in the tumor tissues with vascular invasion corresponded to 47 unique gene products, and the 16 with lower intensities, to 13 unique gene products.

In addition to the protein spots with significant intensity differences between sample groups, we determined the identities of 310 protein spots. The list of the 310 proteins identified, and the peptide data to support protein identification are shown in Supplementary Tables 5 and 6, respectively. The locations of these 310 protein spots are shown in Supplementary Fig. 3.

3.4. Overexpression of CapG in the tumor tissues with vascular invasion

We focused on CapG. The expression level of CapG was higher in the tumor tissues with vascular invasion than in those without (Fig. 4); however, there were no significant differences observed between the tumor and non-tumor tissues (Fig. 3). These observations suggest that CapG is specifically associated with the progression of the cancer rather than carcinogenesis in HCC. In a previous proteomic study, we found that the expression of CapG was correlated with a poor response to treatment with gemcitabine in cholangiocarcinoma, and confirmed its prognostic usefulness by immunohistochemical analysis; the patients with CapG-positive primary tumors had worse prognoses than those who did not [15]. CapG overexpression has been reported in a range of malignancies [16–21]. However, an association between CapG expression and vascular invasion in HCC had not yet been reported. These observations led us to further examine the expression of CapG in HCC.

3.5. Validation of the expression levels of CapG using antibodies .

We validated the expression of CapG using western blotting with 2 specific antibodies against CapG to confirm the results of the 2D-DIGE experiments. Using both antibodies, the expression level of CapG was seen to be significantly higher in the tumor tissues with vascular invasion than in those without vascular invasion and in the non-tumor liver tissues (Fig. 5). In contrast, no significant differences were observed between the non-tumor tissues and tumor tissues (Fig. 5). Overall, these results were consistent with those obtained by 2D-DIGE.

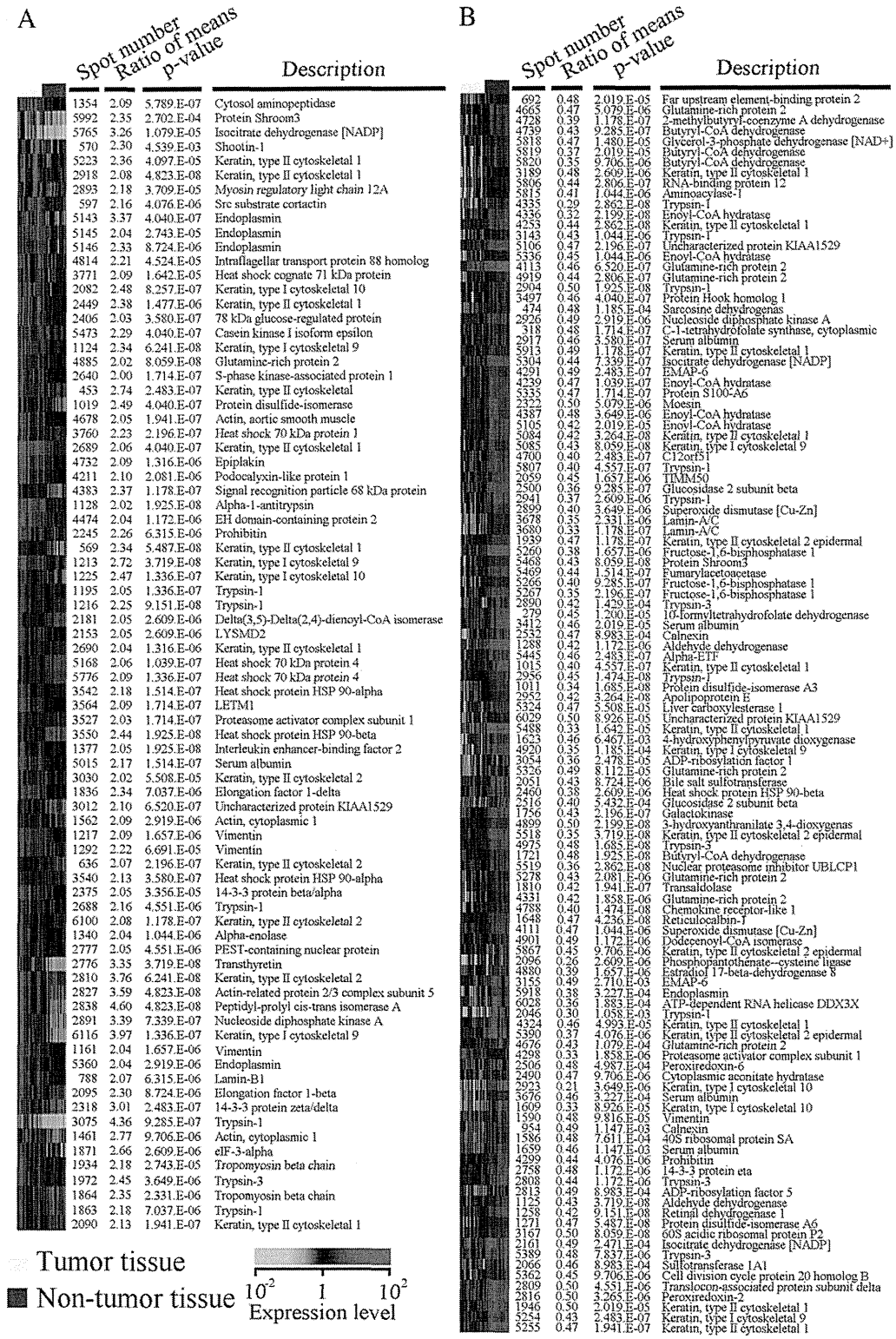

Fig. 3 – One hundred and ninety-seven protein spots with differing intensities between the tumor and non-tumor tissue groups. The ratio of means was calculated by dividing the average intensity of the tumor tissue samples with those of the non-tumor tissue samples. A: Data of 80 protein spots with higher intensities in the tumor tissue sample group are summarized. B: Data of 117 protein spots with lower intensities in the tumor tissue sample groups are summarized. The localization of these protein spots is shown in Supplementary Fig. 1, and the detailed data for protein identification is shown in Supplementary Tables 3 and 4.

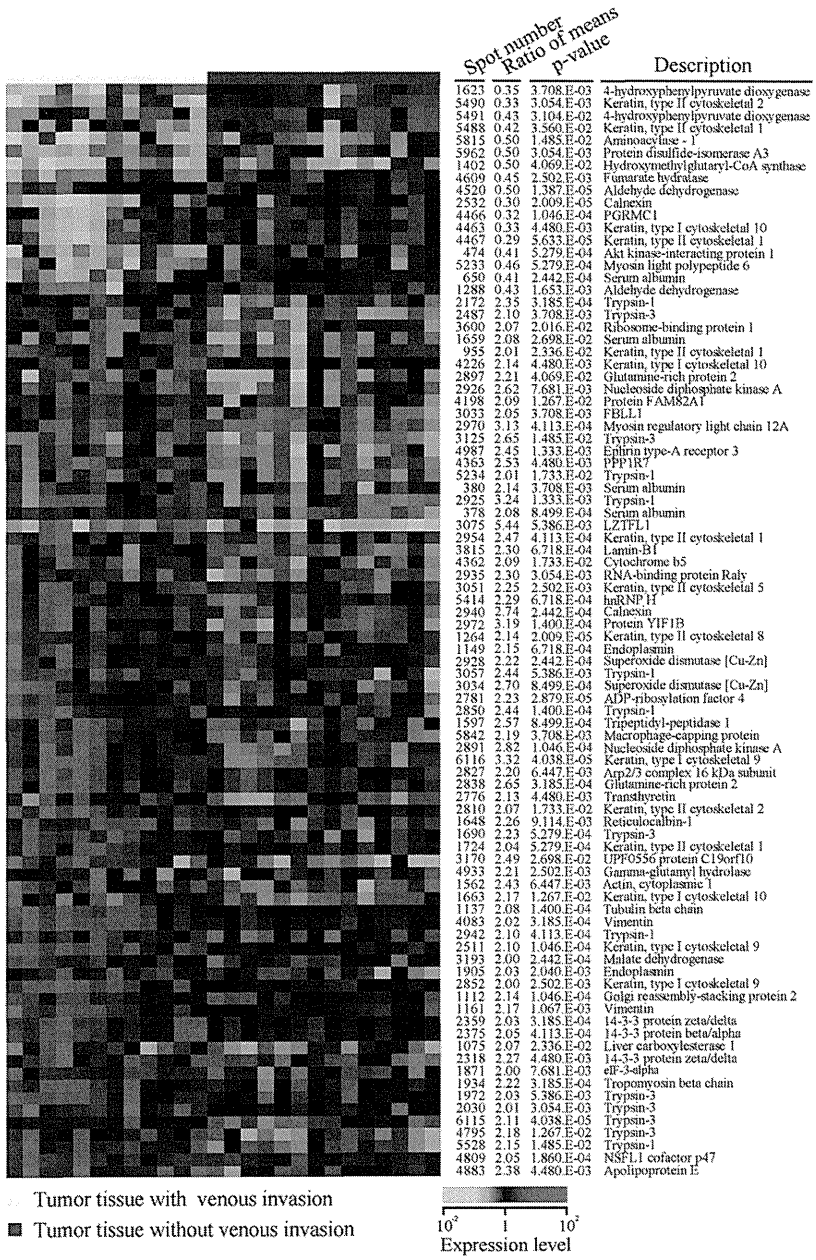

Fig. 4 – Protein spots with differing intensities between tumors with vascular invasion and those without. The ratio of means was calculated by dividing the average intensities of the samples of tumor tissues with vascular invasion with those with no vascular invasion. The localization of these protein spots is shown in Supplementary Fig. 2, and the detailed data for protein identification are shown in Supplementary Tables 5 and 6.

3.6. *Functional significance of CapG overexpression in tumor cells*

To examine the functional significance of the upregulation of CapG in the tumor cells, we examined the effects of CapG silencing on the malignant potential of liver cancer cells. Western blotting showed that CapG silencing was achieved by siRNA transfection (Fig. 6A). The invasion potential was remarkably inhibited by CapG silencing (Fig. 6B and C). In contrast, cell proliferation was not affected by CapG silencing by siRNA transfection (Fig. 6D).

4. Discussion

Prediction of early recurrence is critically important for risk-stratification therapy in HCC. The patients who experience recurrence within 1 year following curative resection have poor prognosis compared to that of others [1]. Various anti-cancer drugs are used to prevent recurrence after surgical resection of HCC [4–9]. The therapeutic strategy is improved by selecting patients who are most likely to have early recurrence after surgery. Alternatively, it may be possible to

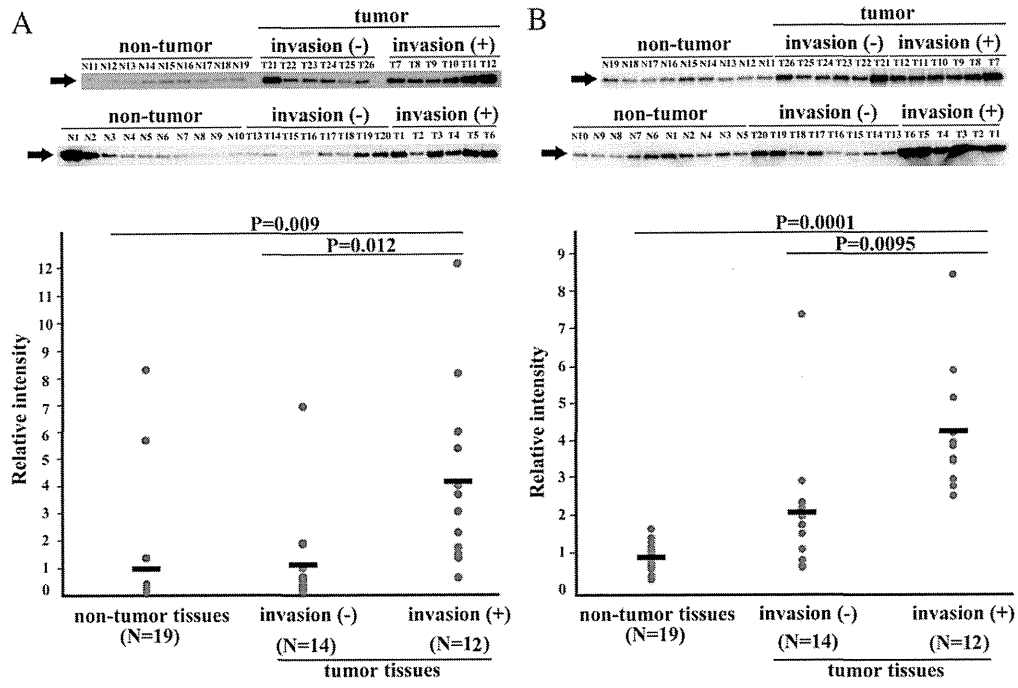

Fig. 5 – Validation of CapG expression by western blotting. CapG expression was examined in the samples used for the 2D-DIGE experiments by using specific antibodies against CapG. Rabbit and chicken antibodies against CapG were used in A and B, respectively. The upper panels show the western blot image, and the lower panels show the results of the quantitative analysis of the western blot data. Note that the expression level of CapG was equivalent between non-tumor and tumor tissues and was significantly different between the tumor tissues from the patients with and without vascular invasion.

avoid seriously invasive treatment in patients whose prognosis is expected to be poor even after extensive treatment. Vascular invasion reflects the invasiveness of HCC and has been considered as an independent risk factor for early recurrence and poor prognosis in HCC [2,22–24]. Therefore, understanding the molecular mechanisms underlying vascular invasion will lead to the development of novel therapies and will eventually benefit patients with HCC.

We identified the association of a higher expression level of CapG with vascular invasion in surgically resected tissues by using a proteomic approach. CapG was originally identified as the protein that binds to the morphologically defined barbed end of actin filaments [25]. Overexpression of CapG is highly associated with the malignant features of tumor cells in lung cancer [26,27], cholangiocarcinoma [15], colorectal cancer [28], breast cancer [21,29,30], ovarian cancer [31], oral cancer [20], and pancreatic cancer [17]. The presence of higher CapG expression in the tumor stroma than in the normal counterpart tissue has also been observed in nasopharyngeal carcinoma [32]. Interestingly, the higher expression of CapG is unique to the tumor margin in the case of breast cancer, suggesting that CapG plays an especially important role in metastasis [29]. In contrast, another study reported that CapG might act as a tumor suppressor gene in stomach cancer, lung cancer, and melanoma [33]. Therefore, the roles of CapG in tumor cells may depend on the type of malignancy. As there have been no reports concerning the expression of CapG in HCC to date, our study will provide further understanding of the molecular mechanisms underlying HCC.

Previous studies have reported the mechanisms underlying the regulation of CapG expression. The activation of tyrosine kinases [34], hypoxia-inducible factor 1 (HIF1) [35], integrin [36], and AP-1 [37] causes upregulation of CapG. The aberrant expression of these proteins has been reported in HCC and is correlated with a poor clinical outcome [38–41]. These proteins may regulate CapG expression in a coordinated manner and contribute to the progression of the HCC. It is worth investigating whether the overexpression of CapG directly promotes the vascular invasion or functions as one of the components of protein network for malignant features.

We found that CapG silencing resulted in reduced invasion but not growth inhibition of the cells. These observations were similar to the results observed in a previous study, wherein Tonack et al. reported that the overexpression of CapG induced enhanced motility but did not induce any changes in cellular proliferation in pancreatic cancer cells [42]. CapG may contribute to venous invasion only by promoting the invasiveness of tumor cells, and there may be the other proteins which upregulate cell proliferation and promote invasion in a coordinate manner with CapG.

Higher expression levels of CapG have been found to be related to malignant features of tumor cells, and the clinical usefulness of CapG suggests that it should form part of the approach for lung cancer [27,43], cholangiocarcinoma [15], colorectal cancer [28,43], ovarian cancer [31], and pancreatic cancer treatments [17]. In this study, we were unable to reproduce the correlation between CapG expression and cancer progression by immunohistochemical analysis using

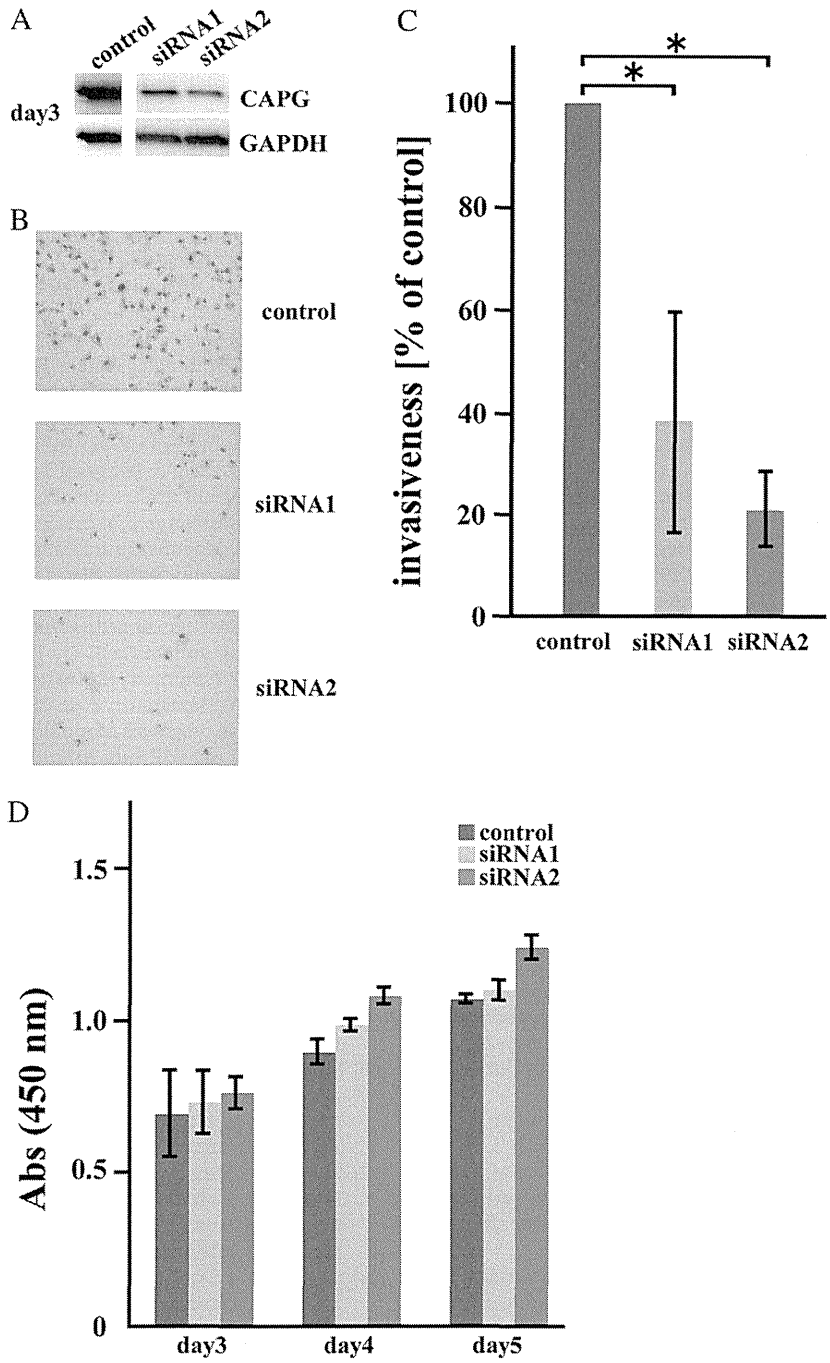

Fig. 6 – Functional assessment of CapG in liver cancer cells in vitro. A: Western blotting showed that the expression of CapG was markedly diminished by transfection with siRNAs (siRNA1 and 2) for CapG. B: Cell growth was not affected by transfection with siRNAs (siRNA1 and 2) for CapG. C: The appearance of liver cancer cells after transfection with the control, siRNA1, and siRNA2. The number of invasive cells decreased after transfection with siRNAs (siRNA1 and 2). D: Quantitative results of the invasion assay. Note that the silencing of CapG by siRNA resulted in a significant reduction of the invasive potential of liver cancer cells.

the antibodies for western blotting (Fig. 5) (data not shown), and the clinical usefulness of CapG in HCC remains to be challenged. The antibody suitable for immunochemical validation will be key to the prognostic and predictive applications of CapG. It is worth considering the information in the antibody databases such as the Human Protein Atlas (www.proteinatlas.org) and the Antibodypedia (www.antibodypedia.com) for the further immunohistochemical validation studies.

Supplementary data to this article can be found online at http://dx.doi.org/10.1016/j.jprot.2012.10.004.

Acknowledgments

This study was supported by the National Cancer Center Research Core Facility and by the National Cancer Center Research and Development Fund (23-A-8 and 23-A-10).

REFERENCES

[1] Thorgeirsson SS, Grisham JW. Molecular pathogenesis of human hepatocellular carcinoma. Nat Genet 2002;31:339-46.
[2] Poon RT, Fan ST, Ng IO, Lo CM, Liu CL, Wong J. Different risk factors and prognosis for early and late intrahepatic recurrence after resection of hepatocellular carcinoma. Cancer 2000;89:500-7.
[3] el-Assal ON, Yamanoi A, Soda Y, Yamaguchi M, Yu L, Nagasue N. Proposal of invasiveness score to predict recurrence and survival after curative hepatic resection for hepatocellular carcinoma. Surgery 1997;122:571-7.
[4] Monaco AP. The role of mTOR inhibitors in the management of posttransplant malignancy. Transplantation 2009;87:157-63.
[5] Feng YX, Wang T, Deng YZ, Yang P, Li JJ, Guan DX, et al. Sorafenib suppresses postsurgical recurrence and metastasis of hepatocellular carcinoma in an orthotopic mouse model. Hepatology 2011;53:483-92.
[6] Mazzaferro V, Romito R, Schiavo M, Mariani L, Camerini T, Bhoori S, et al. Prevention of hepatocellular carcinoma recurrence with alpha-interferon after liver resection in HCV cirrhosis. Hepatology 2006;44:1543-54.
[7] Qu LS, Jin F, Huang XW, Shen XZ. Interferon-alpha therapy after curative resection prevents early recurrence and improves survival in patients with hepatitis B virus-related hepatocellular carcinoma. J Surg Oncol 2010;102:796-801.
[8] Shimizu M, Takai K, Moriwaki H. Strategy and mechanism for the prevention of hepatocellular carcinoma: phosphorylated retinoid X receptor alpha is a critical target for hepatocellular carcinoma chemoprevention. Cancer Sci 2009;100:369-74.
[9] Wang SM, Zhu J, Pan LF, Liu YK. Inhibitory effect of dimeric beta peptide on the recurrence and metastasis of hepatocellular carcinoma in vitro and in mice. World J Gastroenterol 2008;14:3054-8.
[10] Yokoo H, Kondo T, Okano T, Nakanishi K, Sakamoto M, Kosuge T, et al. Protein expression associated with early intrahepatic recurrence of hepatocellular carcinoma after curative surgery. Cancer Sci 2007;98:665-73.
[11] Orimo T, Ojima H, Hiraoka N, Saito S, Kosuge T, Kakisaka T, et al. Proteomic profiling reveals the prognostic value of adenomatous polyposis coli-end-binding protein 1 in hepatocellular carcinoma. Hepatology 2008;48:1851-63.
[12] Budhu A, Forgues M, Ye QH, Jia HL, He P, Zanetti KA, et al. Prediction of venous metastases, recurrence, and prognosis in hepatocellular carcinoma based on a unique immune response signature of the liver microenvironment. Cancer Cell 2006;10:99–111.
[13] Wong CM, Wong CC, Lee JM, Fan DN, Au SL, Ng IO. Sequential alterations of miRNA expression in hepatocellular carcinoma development and venous metastasis. Hepatology 2012;55: 1453-61.
[14] Kondo T, Hirohashi S. Application of highly sensitive fluorescent dyes (CyDye DIGE Fluor saturation dyes) to laser microdissection and two-dimensional difference gel electrophoresis (2D-DIGE) for cancer proteomics. Nat Protoc 2007;1:2940-56.
[15] Morofuji N, Ojima H, Onaya H, Okusaka T, Shimada K, Sakamoto Y, et al. Macrophage-capping protein as a tissue biomarker for prediction of response to gemcitabine treatment and prognosis in cholangiocarcinoma. J Proteomics 2012;75:1577-89.
[16] Dahl E, Sadr-Nabavi A, Klopocki E, Betz B, Grube S, Kreutzfeld R, et al. Systematic identification and molecular characterization of genes differentially expressed in breast and ovarian cancer. J Pathol 2005;205:21-8.
[17] Thompson CC, Ashcroft FJ, Patel S, Saraga G, Vimalachandran D, Prime W, et al. Pancreatic cancer cells overexpress gelsolin family-capping proteins, which contribute to their cell motility. Gut 2007;56:95–106.
[18] Lal A, Lash AE, Altschul SF, Velculescu V, Zhang L, McLendon RE, et al. A public database for gene expression in human cancers. Cancer Res 1999;59:5403-7.
[19] Van Ginkel PR, Gee RL, Walker TM, Hu DN, Heizmann CW, Polans AS. The identification and differential expression of calcium-binding proteins associated with ocular melanoma. Biochim Biophys Acta 1998;1448:290-7.
[20] Nomura H, Uzawa K, Ishigami T, Kouzu Y, Koike H, Ogawara K, et al. Clinical significance of gelsolin-like actin-capping protein expression in oral carcinogenesis: an immunohistochemical study of premalignant and malignant lesions of the oral cavity. BMC Cancer 2008;8:39.
[21] Renz M, Betz B, Niederacher D, Bender HG, Langowski J. Invasive breast cancer cells exhibit increased mobility of the actin-binding protein CapG. Int J Cancer 2008;122:1476-82.
[22] Utsunomiya T, Shimada M, Taguchi KI, Hasegawa H, Yamashita Y, Hamatsu T, et al. Clinicopathologic features and postoperative prognosis of multicentric small hepatocellular carcinoma. J Am Coll Surg 2000;190:331-5.
[23] Paquet KJ, Gad HA, Lazar A, Koussouris P, Mercado MA, Heine WD, et al. Analysis of factors affecting outcome after hepatectomy of patients with liver cirrhosis and small hepatocellular carcinoma. Eur J Surg 1998;164:513-9.
[24] Schoniger-Hekele M, Muller C, Kutilek M, Oesterreicher C, Ferenci P, Gangl A. Hepatocellular carcinoma in Central Europe: prognostic features and survival. Gut 2001;48:103-9.
[25] Casella JF, Maack DJ, Lin S. Purification and initial characterization of a protein from skeletal muscle that caps the barbed ends of actin filaments. J Biol Chem 1986;261: 10915-21.
[26] Shao F, Zhang R, Don L, Ying K. Overexpression of gelsolin-like actin-capping protein is associated with progression of lung adenocarcinoma. Tohoku J Exp Med 2011;225:95–101.
[27] Zhu WY, Hunag YY, Liu XG, He JY, Chen DD, Zeng F, et al. Prognostic evaluation of CapG, gelsolin, P-gp, GSTP1, and topo-II proteins in non-small cell lung cancer. Anat Rec (Hoboken) 2012;295:208-14.
[28] Wu JH, Tian XY, Hao CY. The significance of a group of molecular markers and clinicopathological factors in identifying colorectal liver metastasis. Hepatogastroenterology 2011;58:1182-8.
[29] Kang S, Kim MJ, An H, Kim BG, Choi YP, Kang KS, et al. Proteomic molecular portrait of interface zone in breast cancer. J Proteome Res 2010;9:5638-45.
[30] Xu SG, Yan PJ, Shao ZM. Differential proteomic analysis of a highly metastatic variant of human breast cancer cells using two-dimensional differential gel electrophoresis. J Cancer Res Clin Oncol 2010;136:1545-56.
[31] Partheen K, Levan K, Osterberg L, Claesson I, Fallenius G, Sundfeldt K, et al. Four potential biomarkers as prognostic factors in stage III serous ovarian adenocarcinomas. Int J Cancer 2008;123:2130-7.
[32] Li MX, Xiao ZQ, Chen YH, Peng F, Li C, Zhang PF, et al. Proteomic analysis of the stroma-related proteins in nasopharyngeal carcinoma and normal nasopharyngeal epithelial tissues. Med Oncol 2010;27:134-44.
[33] Watari A, Takaki K, Higashiyama S, Li Y, Satomi Y, Takao T, et al. Suppression of tumorigenicity, but not anchorage

independence, of human cancer cells by new candidate tumor suppressor gene CapG. Oncogene 2006;25:7373-80.
[34] Pierce A, Unwin RD, Evans CA, Griffiths S, Carney L, Zhang L, et al. Eight-channel iTRAQ enables comparison of the activity of six leukemogenic tyrosine kinases. Mol Cell Proteomics 2008;7:853-63.
[35] Liao SH, Zhao XY, Han YH, Zhang J, Wang LS, Xia L, et al. Proteomics-based identification of two novel direct targets of hypoxia-inducible factor-1 and their potential roles in migration/invasion of cancer cells. Proteomics 2009;9: 3901-12.
[36] Chen M, Sinha M, Luxon BA, Bresnick AR, O'Connor KL. Integrin alpha6beta4 controls the expression of genes associated with cell motility, invasion, and metastasis, including S100A4/metastasin. J Biol Chem 2009;284:1484-94.
[37] Bahassi el M, Karyala S, Tomlinson CR, Sartor MA, Medvedovic M, Hennigan RF. Critical regulation of genes for tumor cell migration by AP-1. Clin Exp Metastasis 2004;21: 293-304.
[38] Huynh H, Ong RW, Li PY, Lee SS, Yang S, Chong LW, et al. Targeting receptor tyrosine kinase pathways in hepatocellular carcinoma. Anticancer Agents Med Chem 2011;11:560-75.
[39] Kong J, Pan B, Ke S, Dong S, Li X, Zhou A, et al. Insufficient radiofrequency ablation promotes angiogenesis of residual hepatocellular carcinoma via HIF-1alpha/VEGFA. PLoS One 2012;7:e37266.
[40] Bergamini C, Sgarra C, Trerotoli P, Lupo L, Azzariti A, Antonaci S, et al. Laminin-5 stimulates hepatocellular carcinoma growth through a different function of alpha6beta4 and alpha3beta1 integrins. Hepatology 2007;46: 1801-9.
[41] Guo LL, Xiao S, Guo Y. Activation of transcription factors NF-kappaB and AP-1 and their relations with apoptosis associated-proteins in hepatocellular carcinoma. World J Gastroenterol 2005;11:3860-5.
[42] Tonack S, Patel S, Jalali M, Nedjadi T, Jenkins RE, Goldring C, et al. Tetracycline-inducible protein expression in pancreatic cancer cells: effects of CapG overexpression. World J Gastroenterol 2011;17:1947-60.
[43] Zheng Z, Li J, He X, Chen X, Yu B, Ji J, et al. Involvement of RhoGDI2 in the resistance of colon cancer cells to 5-fluorouracil. Hepatogastroenterology 2010;57:1106-12.

Cancer Cell
Article

Ablation of Fbxw7 Eliminates Leukemia-Initiating Cells by Preventing Quiescence

Shoichiro Takeishi,[1,2] Akinobu Matsumoto,[1,2] Ichiro Onoyama,[1,2] Kazuhito Naka,[3] Atsushi Hirao,[2,3] and Keiichi I. Nakayama[1,2,*]

[1]Department of Molecular and Cellular Biology, Medical Institute of Bioregulation, Kyushu University, 3-1-1 Maidashi, Higashi-ku, Fukuoka, Fukuoka 812-8582, Japan

[2]CREST (Core Research for Evolutional Science and Technology), Japan Science and Technology Agency, Kawaguchi, Saitama 332-0012, Japan

[3]Division of Molecular Genetics, Center for Cancer and Stem Cell Research, Cancer Research Institute, Kanazawa University, Kakuma-machi, Kanazawa, Ishikawa 920-1192, Japan

*Correspondence: nakayak1@bioreg.kyushu-u.ac.jp

http://dx.doi.org/10.1016/j.ccr.2013.01.026

SUMMARY

Imatinib eradicates dividing progenitor cells of chronic myeloid leukemia (CML) but does not effectively target nondividing leukemia-initiating cells (LICs); thus, the disease often relapse after its discontinuation. We now show that Fbxw7 plays a pivotal role in maintenance of quiescence in LICs of CML by reducing the level of c-Myc. Abrogation of quiescence in LICs by Fbxw7 ablation increased their sensitivity to imatinib, and the combination of Fbxw7 ablation with imatinib treatment resulted in a greater depletion of LICs than of normal hematopoietic stem cells in mice. Purging of LICs by targeting Fbxw7 to interrupt their quiescence and subsequent treatment with imatinib may thus provide the basis for a promising therapeutic approach to CML.

INTRODUCTION

Cancer-initiating cells (CICs) are thought to constitute a minor subpopulation of cancer cells that is required for the initiation and maintenance of cancer (Clevers, 2011; Huntly and Gilliland, 2005). This notion is based largely on the characterization of leukemia-initiating cells (LICs), a rare subpopulation of cells that propagates leukemia (Lapidot et al., 1994). LICs were recently shown to share many properties, including self-renewal, pluripotency, and quiescence, with normal hematopoietic stem cells (HSCs) (Clevers, 2011; Huntly and Gilliland, 2005). A fundamental problem in treating leukemia is that the quiescent LIC subpopulation is particularly resistant to conventional chemotherapy and radiation, both of which target cells undergoing DNA replication and are therefore not effective against quiescent (noncycling) cells (Clevers, 2011; Huntly and Gilliland, 2005). Failure to eradicate quiescent LICs may result in reinitiation of malignancy after a period of latency. The development of therapeutic approaches that target quiescent CICs might therefore be expected to have a profound impact on cancer eradication.

Chronic myeloid leukemia (CML) in humans is characterized by the presence of the Philadelphia chromosome, which is generated by a chromosomal translocation that joins the *BCR* gene on chromosome 22 to the *ABL* gene on chromosome 9 (de Klein et al., 1982; Rowley, 1973). CML is a biphasic myeloproliferative disorder, which initially assumes a chronic phase before progressing to an accelerated phase and finally to blast crisis. Given that individuals with CML in blast crisis have a poor prognosis associated with a short survival time, it is critical to treat CML patients during the chronic phase. Several lines

Significance

Most cancer-initiating cells (CICs) are quiescent and therefore resistant to anticancer drugs that preferentially target dividing cells. CICs that survive therapy are a potential cause of relapse. Elucidation of the mechanism by which CICs maintain quiescence is thus critical for the elimination of cancer. Here, we show that Fbxw7 plays a pivotal role in maintenance of quiescence in leukemia-initiating cells (LICs) of chronic myeloid leukemia. Our findings reveal that ablation of Fbxw7 in LICs results in deregulated activation of c-Myc and impaired maintenance of quiescence followed by p53-dependent apoptosis and consequent cell exhaustion. Moreover, they provide a rationale for Fbxw7-targeted therapy to sensitize LICs to currently available drugs by interrupting their quiescence, potentially resulting in a substantial survival benefit.

of evidence indicate that LICs of CML emerge as a result of expression of BCR-ABL in normal HSCs (Pear et al., 1998), supporting the notion that CML is a "stem cell disease."

The BCR-ABL fusion protein possesses constitutive tyrosine kinase activity and triggers molecular events that result in the expansion of malignant hematopoiesis (Deininger et al., 2000). The recent development of the tyrosine kinase inhibitor (TKI) imatinib represented a breakthrough in treatment of the chronic phase of CML, resulting in a marked improvement in the prognosis of CML patients (Druker et al., 2001; Kantarjian et al., 2002). The French CML Intergroup Stop Imatinib study recently found that ~40% of CML patients in complete molecular remission for >2 years while on treatment with imatinib did not relapse within 12 months after discontinuation of imatinib treatment (Mahon et al., 2010). However, this observation suggests that LICs of CML persist in more than half of patients treated with imatinib alone, resulting in relapse after discontinuation of imatinib treatment. Several mechanisms of resistance of CML LICs to imatinib therapy have been suggested, including the maintenance of quiescence (Holtz et al., 2007) and the lack of addiction to BCR-ABL in these cells (Corbin et al., 2011). Although more potent TKIs such as nilotinib and dasatinib have been developed, these drugs also do not target quiescent LICs of CML (Copland et al., 2006; Jørgensen et al., 2007). Therapy with these TKIs thus serves to suppress, not to eliminate, the disease. Moreover, quiescence in CML LICs is thought not only to contribute to TKI resistance but also to be essential for their long-term maintenance. Elucidation of the molecular mechanism by which LICs maintain quiescence is therefore expected to provide a basis for the development of approaches to sensitize CML LICs to TKI therapy, thereby allowing efficient eradication of leukemia cells, prevention of relapse, and increased patient survival. Although several key molecules and signaling pathways have been implicated in LIC maintenance (Ito et al., 2008; Naka et al., 2010; Zhao et al., 2007), the mechanism by which LICs maintain quiescence has been poorly understood.

c-Myc is one of the best characterized proteins found to determine the state of cell proliferation or quiescence (Laurenti et al., 2009). Regulation of the abundance of c-Myc is achieved at several levels, one of which is control of protein stability mediated by posttranslational modification. We and others have shown that the F-box protein Fbxw7 (also known as Fbw7, Sel-10, hCdc4, or hAgo), the substrate-recognition subunit of an SCF-type ubiquitin ligase complex, interacts with and mediates the ubiquitylation of c-Myc (Nakayama and Nakayama, 2006). The ubiquitin-dependent degradation of c-Myc mediated by Fbxw7 has been found to be essential for maintenance of the quiescence and reconstitution capacity of normal HSCs (Matsuoka et al., 2008; Reavie et al., 2010; Thompson et al., 2008). Given that LICs share many properties with normal HSCs, we hypothesized that Fbxw7 might also be required for the maintenance of LICs and that the Fbxw7–c-Myc axis might be a promising target for leukemia therapy.

RESULTS

Fbxw7 Is Required for Maintenance of Quiescence in LICs

To examine whether Fbxw7 expression is modulated during leukemogenesis, we first measured the amount of Fbxw7 mRNA at various stages of the differentiation of leukemic cells in a mouse model of CML caused by the human BCR-ABL fusion protein (Pear et al., 1998). For generation of the model, a c-Kit$^+$Sca-1$^+$Lin$^-$ (KSL) fraction of bone marrow cells, which represents immature hematopoietic cells, was infected with a retrovirus encoding both p210$^{BCR-ABL}$ and green fluorescent protein (GFP) and was subsequently transplanted into syngeneic recipients (Figure 1A). Recipient mice developed signs of CML, including decreased activity, weight loss, an increased number of myeloid cells in peripheral blood, and splenomegaly, and all mice died within 4 weeks after transplantation. Bone marrow cells were collected from the recipient mice after they began to show such signs of CML. Reverse transcription (RT) and real-time PCR analysis revealed that Fbxw7 mRNA was highly abundant in the LIC compartment (GFP$^+$KSL population), whereas it was present in much smaller amounts in the leukemic progenitor compartment (GFP$^+$c-Kit$^+$Sca-1$^-$Lin$^-$ population) and its abundance decreased further as cell differentiation progressed (Figure 1B). Similar results were obtained by quantification of the copy number of Fbxw7 mRNA per cell in these various compartments (Figure S1A available online). These data thus suggested that Fbxw7 expression during leukemogenesis is regulated at least in part at the transcriptional level.

We next examined the role of Fbxw7 in the maintenance of LIC quiescence by conditional disruption of the Fbxw7 gene in this CML mouse model. KSL cells from Mx1-Cre;*Fbxw7*$^{+/+}$ (control) and Mx1-Cre;*Fbxw7*$^{F/F}$ mice were infected with the retrovirus encoding BCR-ABL and GFP and were then transplanted into syngeneic wild-type mice. The donor mice harbored wild-type (+) or floxed (F) alleles of *Fbxw7*, as well as a transgene for Cre recombinase under the control of the Mx1 gene promoter. The number of white blood cells in peripheral blood of the recipient mice was determined every 5 days; when it had increased to >20,000/μl, GFP$^+$KSL cells (2×10^4) were collected from the recipients and transplanted into additional recipient mice (first bone marrow transplantation [BMT]). These recipients were then injected with polyinosinic:polycytidylic acid (pIpC) beginning the day after the first BMT to activate the Mx1-Cre transgene and thereby to delete the floxed *Fbxw7* allele in Mx1-Cre;*Fbxw7*$^{F/F}$ leukemia cells (to yield the *Fbxw7*$^{\Delta/\Delta}$ genotype) (Figure 1C). One week after the final injection of pIpC, we confirmed that almost all floxed alleles of *Fbxw7* were inactivated in each fraction of the targeted leukemia cells (Figure S1B). Analysis of the cell cycle status of leukemic cells from the recipients of the first BMT by flow cytometry revealed that the frequency of Hoechst^{low}pyronin Y^{low} cells, which represent cells in G_0 phase (quiescence), was significantly smaller in the GFP$^+$KSL compartment of *Fbxw7*$^{\Delta/\Delta}$ leukemia cells than in the corresponding compartment of pIpC-treated Mx1-Cre;*Fbxw7*$^{+/+}$ (control) leukemia cells (Figure 1D). Given that gene ablation induced by pIpC is mediated by interferon, which has been shown to act directly on HSCs to induce cell cycle progression (Essers et al., 2009), recipients of control bone marrow cells as well as those of Mx1-Cre;*Fbxw7*$^{F/F}$ cells were injected with pIpC to eliminate any bias attributable to interferon action. In contrast to LICs, most cells in the GFP$^+$c-Kit$^+$Sca-1$^-$Lin$^-$ compartment were actively cycling, and the proportion of quiescent cells in this compartment did not differ between the two genotypes (Figure 1D), consistent with our observation that

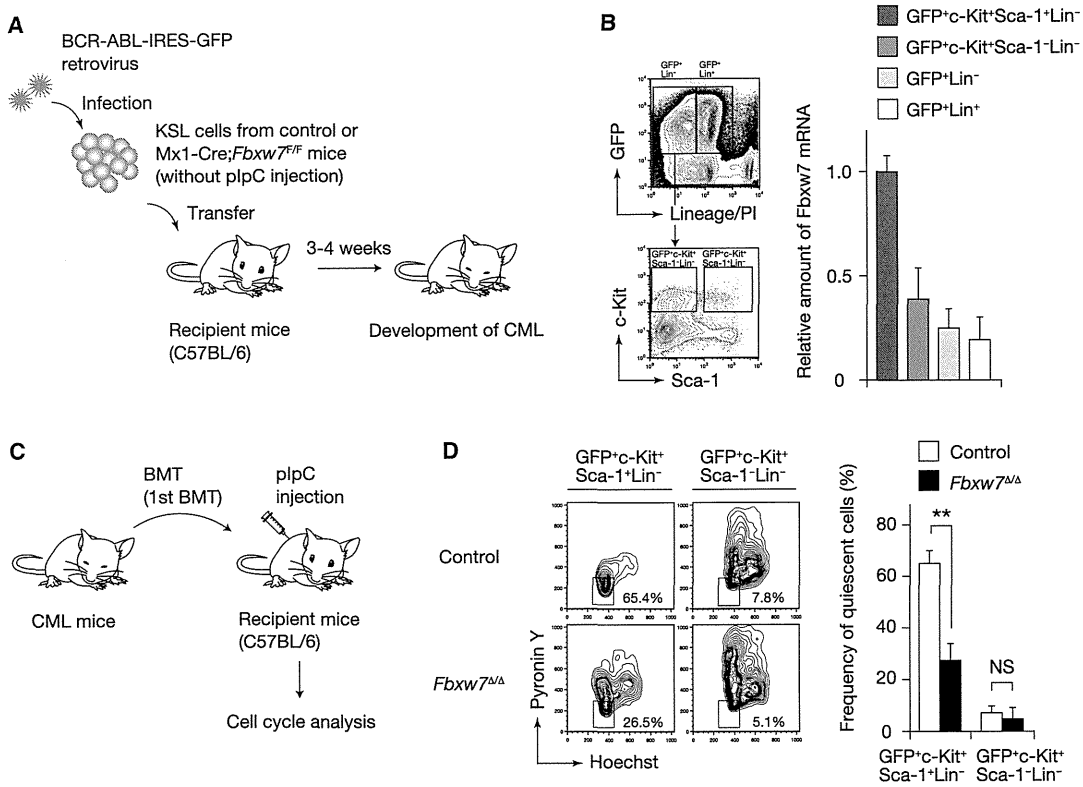

Figure 1. Loss of Fbxw7 in LICs Promotes Cell Cycle Progression

(A) Experimental strategy for generation of a mouse model of CML.

(B) GFP$^+$ cells of control CML bone marrow were fractionated by FACS as indicated (left panels; PI, propidium iodide) and then assayed for Fbxw7 mRNA by RT and real-time PCR analysis (right panel; n = 3).

(C) Experimental strategy for deletion of the floxed *Fbxw7* allele in leukemic cells.

(D) CML bone marrow cells from recipients of the first BMT were subjected to flow cytometry (left panels) for determination of the percentage of quiescent cells in the indicated fractions (right panel; n = 3).

Data are means ± SD. **p < 0.01; NS, not significant. See also Figure S1.

these cells express *Fbxw7* at a low level (Figure 1B). Together, these results suggested that Fbxw7 is expressed predominantly in the LIC fraction of leukemia cells and is required for maintenance of quiescence in LICs.

Fbxw7 Is Required for Leukemic Stemness

The critical role of Fbxw7 in the maintenance of quiescence in LICs and the fact that quiescence is thought to be essential for maintenance of normal HSCs prompted us to examine whether Fbxw7 is essential for LIC maintenance. To test this possibility, we first performed long-term culture-initiating cell assays. Control and *Fbxw7*$^{\Delta/\Delta}$ GFP$^+$KSL cells were isolated from recipients of the first BMT, cultured on OP-9 stromal cells for 2 or 6 weeks, and then subjected to colony-formation assays (Figure 2A). In these assays, the number of colony-forming cells arising after short-term culture (2 weeks) on OP-9 cells mainly reflects progenitor function, whereas that arising after long-term culture (6 weeks) reflects stem cell function (Matsumoto et al., 2011b). We confirmed that the floxed alleles of *Fbxw7* were indeed inactivated efficiently in the *Fbxw7*$^{\Delta/\Delta}$ leukemic cells cultured on OP-9 cells (Figure S2A). The number of cells derived from *Fbxw7*$^{\Delta/\Delta}$ GFP$^+$KSL cells during culture on OP-9 cells was smaller than that derived from the corresponding control cells (Figure S2B). Furthermore, whereas the number of colonies derived from the cells cultured for the short term (2 weeks) did not differ between the two genotypes (Figure 2B), the number of colonies formed by *Fbxw7*$^{\Delta/\Delta}$ GFP$^+$KSL cells was significantly smaller than that formed by the control cells after long-term culture (6 weeks), suggesting that increased cycling of *Fbxw7*$^{\Delta/\Delta}$ LICs eventually results in their exhaustion. We also performed serial replating assays and confirmed that almost all floxed alleles of *Fbxw7* were inactivated in the targeted leukemic cells after serial replating (Figure S2C). Whereas the number of colonies formed did not differ between control and Fbxw7-deficient LICs in the first plating, the number of colonies derived from Fbxw7-deficient LICs was significantly smaller than that derived from control LICs in the second plating (Figure S2D).

To assess the repopulating ability of *Fbxw7*$^{\Delta/\Delta}$ LICs in vivo, we performed serial BMT experiments in which we collected control and *Fbxw7*$^{\Delta/\Delta}$ GFP$^+$KSL cells (2 × 10^4) from the recipients of the first BMT and transplanted these cells into new recipients (second BMT) (Figure 2C). Almost all floxed alleles of *Fbxw7* were inactivated in the targeted leukemic cells isolated from the recipients of the second BMT (Figure S2E). Whereas the

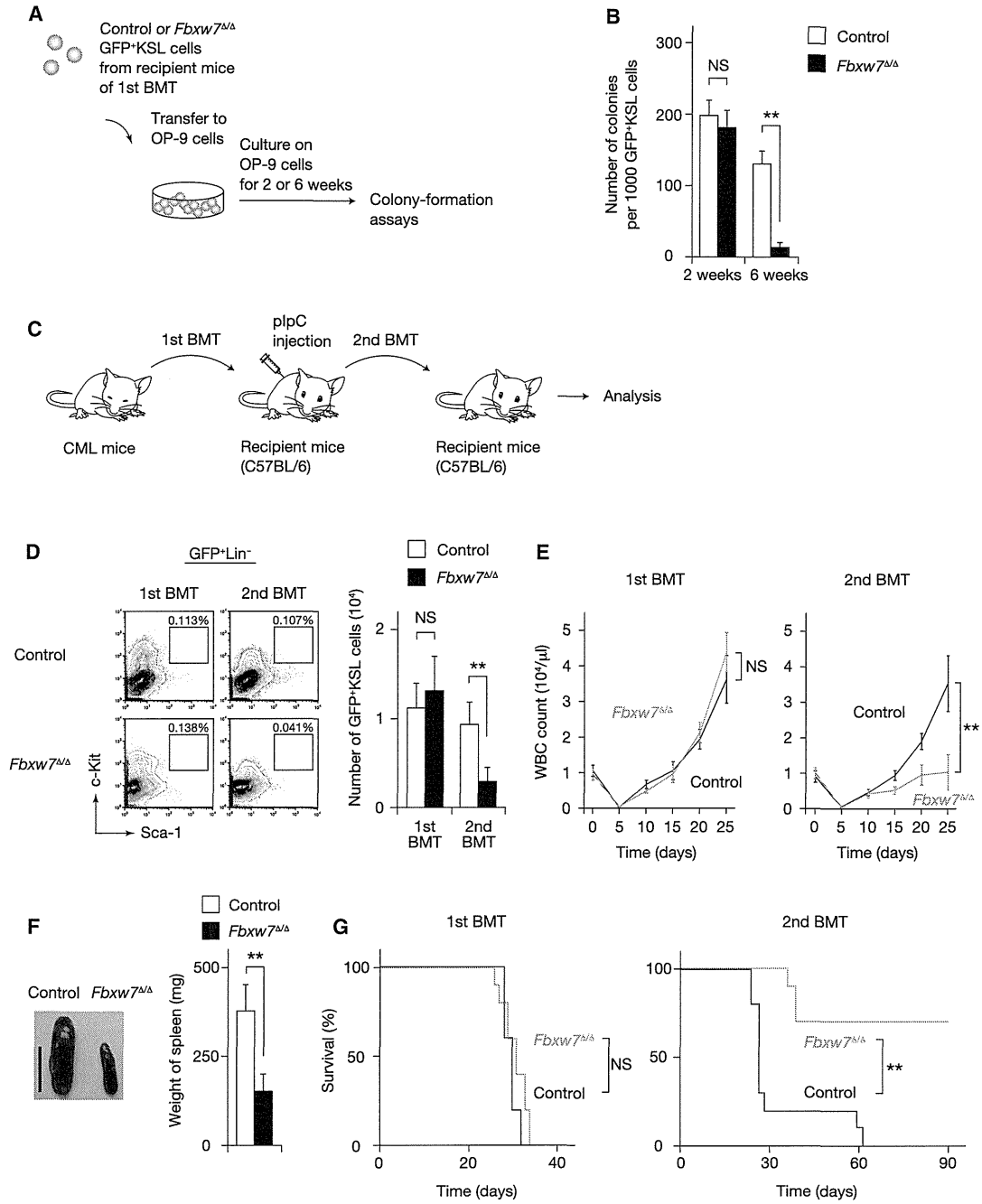

Figure 2. Loss of Fbxw7 in LICs Results in Cell Exhaustion

(A) Experimental strategy for colony formation assays.

(B) Colony formation by BCR-ABL-transduced KSL cells of the indicated genotypes after 2 or 6 weeks of culture on OP-9 cells (n = 3).

(C) Experimental strategy for serial BMT experiments.

(D) Flow-cytometric determination of the absolute number of GFP$^+$KSL cells in bone marrow of recipients (n = 5) after the first and second BMTs.

(E) Numbers of white blood cells (WBC) in peripheral blood of recipient mice (n = 10) after the first and second BMTs.

(F) Representative appearance (scale bar, 10 mm) and weight (n = 5) of the spleen in recipients of the second BMT.

(G) Survival of recipient mice (n = 10) after the first and second BMTs.

Data are means ± SD. **$p < 0.01$; NS, not significant. See also Figure S2.

number of GFP$^+$KSL cells isolated from recipients of the first BMT did not differ between the two genotypes, that of GFP$^+$KSL cells isolated from recipients of the second BMT was greatly reduced in the case of *Fbxw7*$^{\Delta/\Delta}$ donor cells compared with that for control donor cells (Figure 2D). These results thus suggested that the loss of Fbxw7 results in disruption of quiescence, followed by eventual exhaustion of LICs. We also observed that both the proportion and absolute number of Fbxw7-deficient leukemic progenitors were significantly smaller than those of control leukemic progenitors in recipients of the second BMT (Figures S2F and S2G). Given that Fbxw7 deficiency did not affect the cell cycle status of the progenitors (Figure 1D), these latter results were likely attributable to a functional defect in Fbxw7-deficient LICs. Consistent with these observations, the timing of CML development did not differ between the two types of recipients of the first BMT (Figure 2E). In contrast, after the second BMT, Fbxw7 deficiency prevented the propagation of leukemic cells in peripheral blood (Figure 2E) and the spleen (Figure 2F). Furthermore, whereas most recipients of control LICs died of CML at ~30 days after the second BMT, ~70% of mice receiving *Fbxw7*$^{\Delta/\Delta}$ LICs survived for >120 days (Figure 2G; data not shown). In a similar mouse model of CML, LICs were also shown to give rise to acute lymphocytic leukemia (ALL) with a long latency (Pear et al., 1998). Notably, we did not observe development of ALL or CML in recipients of *Fbxw7*$^{\Delta/\Delta}$ LICs later than 40 days after the second BMT. Flow cytometric analysis and histological examination revealed the almost complete absence of leukemic cells in peripheral blood and no infiltration of leukemic cells in the spleen, liver, or lungs of the recipients of Fbxw7-deficient LICs that survived for >90 days after the second BMT (Figure S2H), suggesting that Fbxw7-deficient LICs lose their potential to generate malignancies. Fbxw7 thus appears to be essential for the long-term maintenance of leukemia-initiating potential.

Accumulation of c-Myc Is Responsible for Loss of Leukemic Stemness

We next investigated the mechanism underlying LIC exhaustion associated with Fbxw7 deficiency. Fbxw7 targets many proteins related to HSC maintenance, including c-Myc, Notch1 intracellular domain (NICD1), and mammalian target of rapamycin (mTOR) (Nakayama and Nakayama, 2006). To determine whether these substrates accumulate in Fbxw7-deficient LICs, we examined their abundance in LICs isolated from recipients of the first BMT and found that the abundance of c-Myc was increased in *Fbxw7*$^{\Delta/\Delta}$ GFP$^+$KSL cells compared with control GFP$^+$KSL cells (Figure 3A). In contrast, the expression levels of NICD1 and mTOR did not differ between control and Fbxw7-deficient GFP$^+$KSL cells (Figures S3A and S3B).

To determine whether c-Myc accumulation is responsible for the phenotype of *Fbxw7*$^{\Delta/\Delta}$ LICs, we first cultured control and *Fbxw7*$^{\Delta/\Delta}$ GFP$^+$KSL cells isolated from recipients of the first BMT with the c-Myc inhibitor 10058-F4 (Follis et al., 2009). A colony-formation assay performed after culture of GFP$^+$KSL cells for 2 or 6 weeks in the presence of 10058-F4 revealed that the number of colonies did not differ between the two genotypes (Figure 3B). To confirm that 10058-F4 indeed inhibited c-Myc function in these cells, we measured the abundance of mRNAs for cyclin D2 and ornithine decarboxylase 1 (ODC1), the genes for which are direct targets of c-Myc. The abundance of these mRNAs was increased in Fbxw7-deficient LICs compared with that in control cells, and each increase was attenuated by 10058-F4, suggesting that 10058-F4 indeed inhibits c-Myc activity in these cells (Figure 3C). To demonstrate further that c-Myc accumulation contributes to the phenotype of Fbxw7-deficient LICs, we next generated Mx1-Cre;*Fbxw7*$^{F/F}$;*c-Myc*$^{+/F}$ mice in order to analyze the cell cycle status and colony-forming ability of *Fbxw7*$^{\Delta/\Delta}$;*c-Myc*$^{+/\Delta}$ LICs. The loss of quiescence and impaired colony-forming ability apparent for *Fbxw7*-deficient LICs were normalized by the additional deletion of one allele of the c-Myc gene (Figures 3D and 3E). In contrast, neither a γ-secretase inhibitor, *N*-[*N*-(3,5-difluorophenacetyl)-L-alanyl]-*S*-phenylglycine *t*-butyl ester (DAPT), which antagonizes Notch signaling, nor rapamycin, which antagonizes mTOR, mimicked the effects of 10058-F4 or c-Myc depletion (Figures S3C and S3D), suggesting that neither Notch nor mTOR contributes to the phenotype of Fbxw7-deficient LICs. Collectively, these results thus indeed suggested that the phenotype of *Fbxw7*$^{\Delta/\Delta}$ LICs is attributable to increased activity of c-Myc.

We next compared the amount of BCR-ABL between control and Fbxw7-deficient LICs. Immunoblot analysis revealed no substantial difference in the level of BCR-ABL between these cells (Figure S3E). We further examined whether Fbxw7 deficiency affects signaling downstream of BCR-ABL in LICs by analyzing the phosphorylation of Stat5 (on Tyr^{694}), Crkl (on Tyr^{207}), and Akt (on Ser^{473}). Intracellular flow cytometric analysis revealed that the proportions of cells expressing the phosphorylated forms of Stat5 or Crkl were similar for control and Fbxw7-deficient LICs (Figures S3F and S3G). In contrast, the frequency of cells positive for phosphorylated Akt was greater for Fbxw7-deficient LICs than for control LICs (Figure S3H). We previously showed that Akt phosphorylation is inhibited by transforming growth factor–β (TGF-β) signaling in CML LICs (Naka et al., 2010), and a recent study indicated that TGF-β is activated by a niche for HSCs (Yamazaki et al., 2011). These observations suggest that Fbxw7-deficient LICs might enter the cell cycle and cease to interact with a LIC niche, resulting in a decrease in TGF-β signaling and an increase in Akt phosphorylation. Consistent with this notion, we found that the frequency of cells positive for phosphorylated Smad2/3 was smaller for *Fbxw7*$^{\Delta/\Delta}$ GFP$^+$KSL cells than for control cells (Figure S3I). Moreover, TGF-β1 treatment reversed the increase in the proportion of Fbxw7-deficient LICs positive for phosphorylated Akt (Figure S3J), suggesting that downregulation of TGF-β signaling indeed contributes to this increase. Collectively, our results exclude the possibility that the phenotype of Fbxw7-deficient LICs is attributable to downregulation of BCR-ABL itself or of signaling downstream of BCR-ABL.

To further exclude the possibility that Fbxw7 deficiency in LICs impairs their homing ability, we collected the same number of control and *Fbxw7*$^{\Delta/\Delta}$ GFP$^+$KSL cells from recipients of the first BMT, transplanted the cells into new recipient mice, and determined the proportion of GFP$^+$ cells among bone marrow cells by flow cytometry at 12 hr after transplantation. We found that the frequency of GFP$^+$ cells did not differ significantly between the two genotypes (Figure S3K), suggesting that the phenotype of mice receiving Fbxw7-deficient LICs was not likely a consequence of impaired homing.

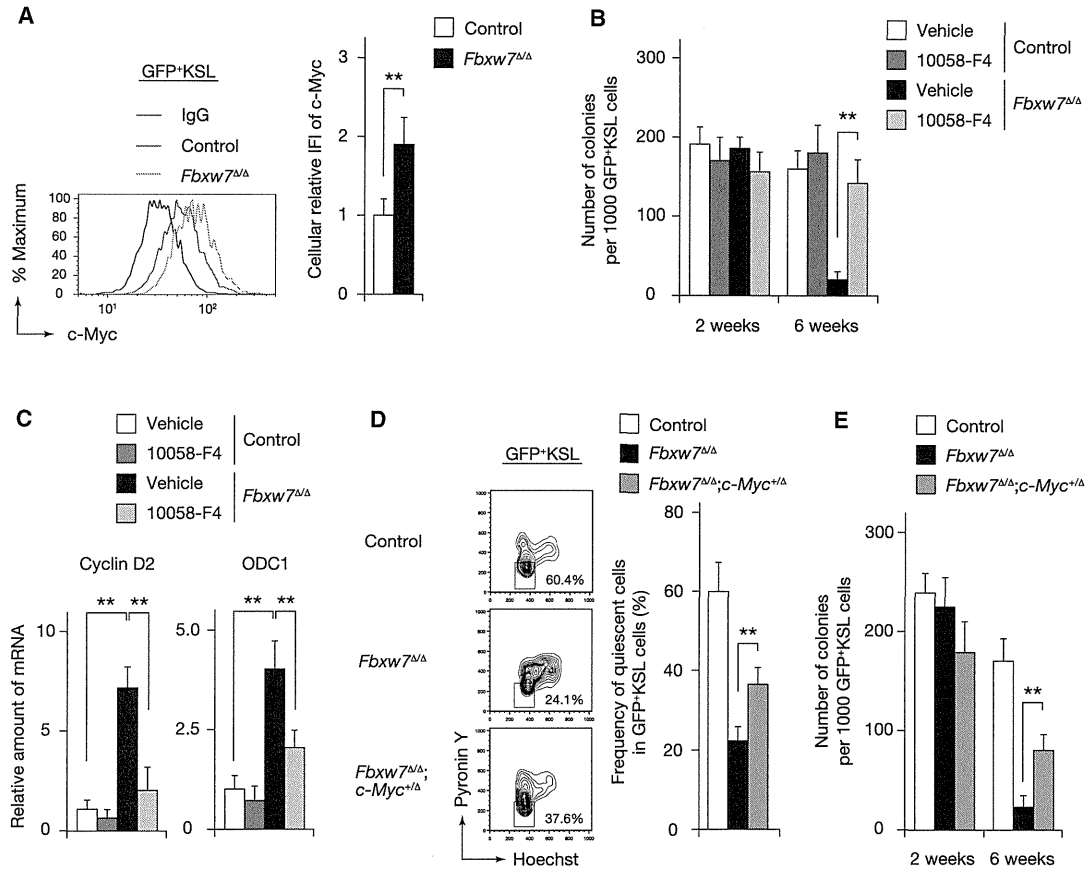

Figure 3. Inhibition of c-Myc Rescues the Phenotype of Fbxw7-Deficient LICs

(A) The abundance of c-Myc in *Fbxw7*$^{\Delta/\Delta}$ or control GFP$^+$KSL cells from mouse recipients of the first BMT was measured by flow cytometry (left panel). Relative c-Myc immunofluorescence intensity (IFI) was determined (n = 5) (right panel). IgG, immunoglobulin G.

(B) Colony formation by *Fbxw7*$^{\Delta/\Delta}$ and control LICs after culture for 2 or 6 weeks with or without 10058-F4 (n = 5).

(C) Control and *Fbxw7*$^{\Delta/\Delta}$ LICs were assayed for cyclin D2 and ODC1 mRNAs by RT and real-time PCR analysis after culture on OP-9 cells for 2 weeks with or without 10058-F4 (n = 5).

(D) The percentage of quiescent cells among GFP$^+$KSL cells was determined for control, *Fbxw7*$^{\Delta/\Delta}$, or *Fbxw7*$^{\Delta/\Delta}$;*c-Myc*$^{+/\Delta}$ bone marrow cells from recipients (n = 5) of the first BMT.

(E) Colony formation by BCR-ABL-transduced KSL cells of the indicated genotypes after 2 or 6 weeks of culture on OP-9 cells (n = 3).

Data are means ± SD. **p < 0.01. See also Figure S3.

Loss of Fbxw7 in LICs Induces Apoptosis in a p53-Dependent Manner

Given that deregulation of c-Myc activation often triggers apoptosis in a p53-dependent manner (Matsuoka et al., 2008; Onoyama et al., 2007), we postulated that p53-dependent apoptosis might be induced by accumulation of c-Myc in Fbxw7-deficient LICs and contribute to LIC exhaustion. The proportion of apoptotic cells did not differ significantly between control and Fbxw7-deficient LICs isolated from recipients of the first BMT. However, the frequency of annexin V$^+$ apoptotic cells was markedly greater among *Fbxw7*$^{\Delta/\Delta}$ GFP$^+$KSL cells than among control GFP$^+$KSL cells from recipients of the second BMT, whereas such a difference was not apparent for leukemic progenitors (Figure 4A). To determine whether this apoptosis in Fbxw7-deficient LICs is induced in a p53-dependent manner, we next cultured control or *Fbxw7*$^{\Delta/\Delta}$ GFP$^+$KSL cells isolated from recipients of the first BMT with the p53 inhibitor pifithrin-α (PFTα) (Komarov et al., 1999). Analysis of colony formation revealed that the exhaustion apparent in *Fbxw7*$^{\Delta/\Delta}$ GFP$^+$KSL cells after 6 weeks of culture was efficiently inhibited by treatment of the cells with PFTα (Figure 4B). To confirm that PFTα indeed inhibits p53 function in these cells, we measured the abundance of mRNAs for p21 and Noxa, the genes for which are direct targets of p53. The amounts of these mRNAs were increased in Fbxw7-deficient LICs compared with those in control cells, and each increase was attenuated by treatment with PFTα (Figure 4C), suggesting that PFTα indeed inhibits p53 activity in these cells. To further show that Fbxw7 deficiency in LICs induces apoptosis in a p53-dependent manner, we generated Mx1-Cre;*Fbxw7*$^{F/F}$;*p53*$^{-/-}$ mice in order to determine the proportion of apoptotic cells and colony-forming ability for *Fbxw7*$^{\Delta/\Delta}$;*p53*$^{-/-}$ LICs. The increase in the frequency of apoptosis apparent for Fbxw7-deficient LICs from recipients of the second BMT was not observed with *Fbxw7*$^{\Delta/\Delta}$;*p53*$^{-/-}$ LICs

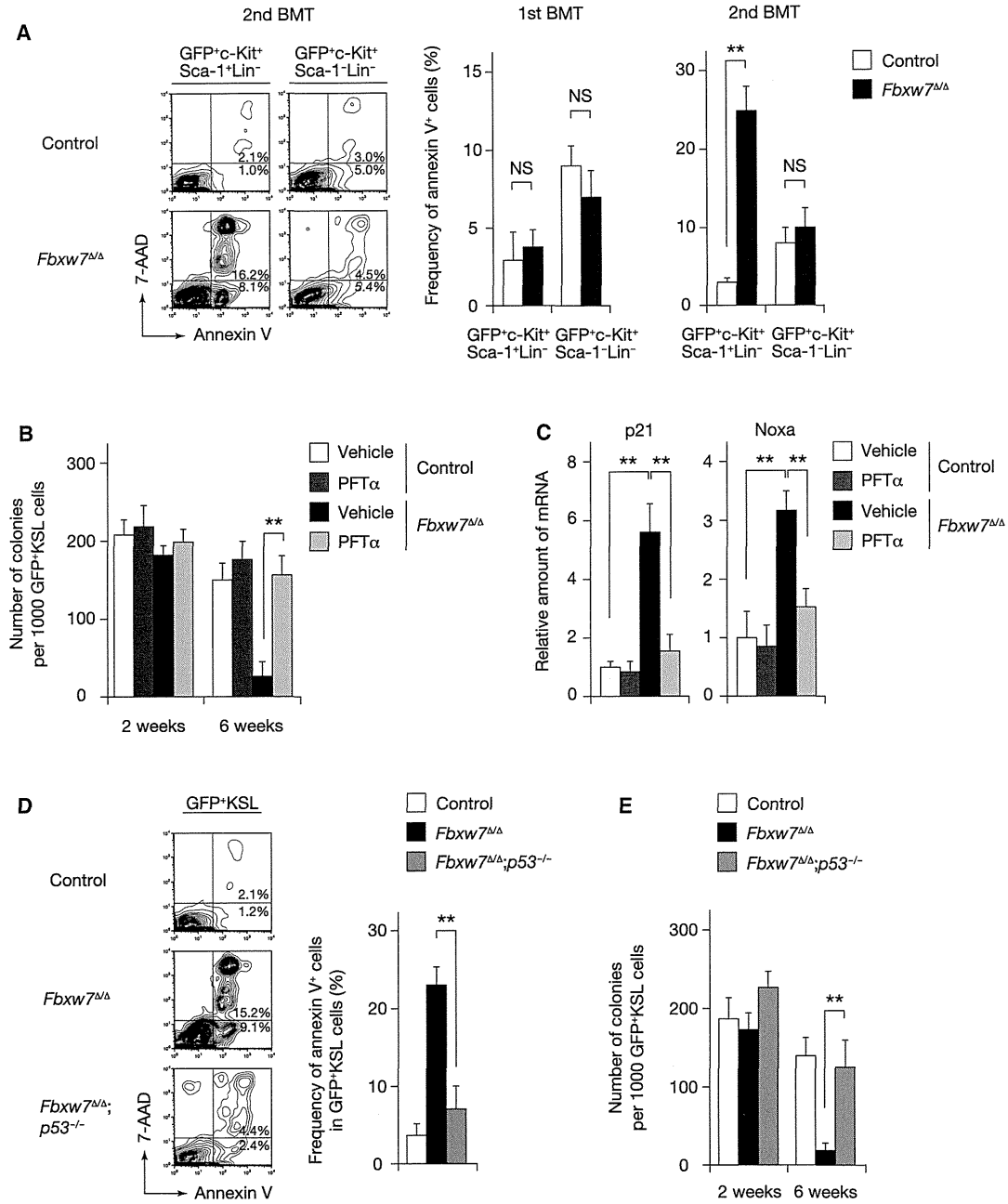

Figure 4. Apoptosis Is Induced in Fbxw7-Deficient LICs in a p53-Dependent Manner

(A) The frequency of annexin V$^+$ cells among *Fbxw7*$^{\Delta/\Delta}$ and control cells of the indicated fractions from mouse recipients (n = 3) of the first or second BMT was determined by flow cytometry. 7-AAD, 7-aminoactinomycin D.

(B) Colony formation by *Fbxw7*$^{\Delta/\Delta}$ and control LICs after culture for 2 or 6 weeks with or without PFTα (n = 5).

(C) Control and *Fbxw7*$^{\Delta/\Delta}$ LICs were assayed for p21 and Noxa mRNAs by RT and real-time PCR analysis after culture on OP-9 cells for 2 weeks with or without PFTα (n = 5).

(D) The proportion of annexin V$^+$ cells among GFP$^+$KSL cells was determined by flow cytometry for control, *Fbxw7*$^{\Delta/\Delta}$, or *Fbxw7*$^{\Delta/\Delta}$;*p53*$^{-/-}$ bone marrow cells from recipients (n = 3) of the second BMT.

(E) Colony formation by cells of the indicated genotypes after culture for 2 or 6 weeks on OP-9 cells (n = 3).

Data are means ± SD. **$p < 0.01$; NS, not significant.

(Figure 4D). Consistent with this finding, the decrease in the number of colonies derived from Fbxw7-deficient LICs after 6 weeks of culture on OP-9 cells was reversed by deletion of the p53 gene (Figure 4E). Collectively, these results indicated that Fbxw7 deficiency in LICs results in deregulated c-Myc activation, impaired maintenance of quiescence, subsequent apoptosis as a result of p53 induction, and consequent cell exhaustion.

The Combination of Fbxw7 Ablation and Anticancer Drug Treatment Is Effective for LIC Eradication

Although our results implicated Fbxw7 as a potential target for leukemia therapy, the timing of CML development and the survival rate did not differ between the recipients of the first BMT harboring control or Fbxw7-deficient LICs (Figures 2E and 2G), suggesting that inhibition of Fbxw7 alone would not suffice as an effective therapy for CML. To address this problem, we examined the effects of combining Fbxw7 ablation with imatinib. Recipients of the first BMT were injected with pIpC on 7 alternate days beginning the day after transplantation and were then administered imatinib twice a day at 100 mg/kg for 2 weeks beginning 20 days after transplantation (Figure 5A). Determination of the proportion of annexin V^+ cells among GFP^+KSL cells revealed that the frequency of apoptosis among imatinib-treated $Fbxw7^{\Delta/\Delta}$ LICs was significantly greater than that among imatinib-treated control LICs (Figure 5B), indicating that Fbxw7-deficient LICs are sensitive to imatinib. In contrast, imatinib was able to efficiently induce apoptosis in both control and Fbxw7-deficient leukemic progenitors and bulk leukemic cells. The number of colonies formed by imatinib-treated $Fbxw7^{\Delta/\Delta}$ GFP^+KSL cells was smaller than that formed by vehicle-treated $Fbxw7^{\Delta/\Delta}$ GFP^+KSL cells or by imatinib-treated control GFP^+KSL cells (Figure 5C).

Analysis of the effects of this combination therapy on CML development in vivo revealed that it markedly reduced the number of Fbxw7-deficient LICs (Figure 5D). Consistent with these findings, most mice treated with imatinib alone showed a moderate delay in the onset of disease but developed CML after discontinuation of imatinib (Figure 5E), dying within 60 days after BMT (Figure 5F). In contrast, combination therapy with Fbxw7 ablation and imatinib resulted in a marked attenuation of CML development that remained apparent even after discontinuation of imatinib treatment (Figures 5E and 5F). Furthermore, when LICs isolated from recipients of the first BMT were transplanted into new recipients, we found that, whereas LICs treated with imatinib alone still had the potential to confer disease, an apparently complete cure was achieved in all recipients of LICs treated with the combination therapy of Fbxw7 ablation and imatinib (Figure 5F). These results indicated that the effectiveness of the combination therapy is attributable to disrupted maintenance of LICs. We also combined *Fbxw7* deletion and treatment with the conventional anticancer drug cytosine arabinoside (Ara-C) and obtained similar results (Figures S4A–S4D). Analysis of signaling downstream of BCR-ABL in GFP^+KSL cells isolated from recipients of the first BMT at 36 days after transplantation revealed no differences in the proportions of cells expressing phosphorylated forms of Stat5, Crkl, or Akt between imatinib-treated control and $Fbxw7^{\Delta/\Delta}$ LICs (Figures S4E–S4G). Collectively, these data thus suggested that LICs whose quiescence is interrupted by Fbxw7 loss are actively cycling and thus sensitive to imatinib or Ara-C treatment and that these combination therapies of Fbxw7 ablation and anticancer drug administration are able to eradicate LICs and provide a survival advantage compared with currently available treatments.

Fbxw7 Deficiency Affects LICs More than It Does Normal HSCs

Given that Fbxw7 is essential for maintenance of both HSCs and LICs, the targeting of LICs by Fbxw7 ablation combined with anticancer drugs might also be expected to damage HSCs. We thus compared the sensitivity of HSCs and LICs to Fbxw7 ablation. To this end, we infected KSL cells from control or Mx1-Cre;$Fbxw7^{F/F}$ mice with the retrovirus encoding the $p210^{BCR-ABL}$ oncoprotein and GFP (to yield LICs) or with a virus encoding GFP alone (to yield HSCs) and then transplanted the cells into recipient mice. GFP^+KSL cells from these mice were subsequently transferred to new recipients, which were then injected with pIpC (Figure 6A). Analysis of GFP^+KSL cells from these latter recipients revealed that exit from quiescence induced by Fbxw7 ablation was more pronounced for LICs than for HSCs (Figure 6B). Accordingly, whereas the proportion of apoptotic cells among LICs did not differ from that among HSCs isolated from recipients of the first BMT, it was greater for Fbxw7-deficient LICs than for Fbxw7-deficient HSCs isolated from recipients of a second BMT (Figure 6C). Consistent with these results, whereas Fbxw7 deficiency did not affect the number of HSCs or LICs in recipients of the first BMT, it reduced the number of LICs to a greater extent than it did that of HSCs in recipients of the second BMT (Figure 6D).

To examine the mechanism underlying this difference in sensitivity to Fbxw7 deficiency between HSCs and LICs, we first compared the amount of Fbxw7 mRNA in these cells. RT and real-time PCR analysis revealed that the abundance of Fbxw7 mRNA in LICs was more than twice that in HSCs (Figure S5A). Given that such an increase in the amount of Fbxw7 mRNA was not observed in KSL cells expressing a kinase-dead (K1176R) mutant of BCR-ABL (Zhang and Ren, 1998), the upregulation of Fbxw7 mRNA in LICs is likely attributable to BCR-ABL kinase activity. The level of c-Myc mRNA was also markedly increased in LICs compared with that in HSCs or in KSL cells expressing the kinase-dead mutant of BCR-ABL (Figure S5B), and intracellular flow cytometric analysis revealed that the abundance of c-Myc in LICs was about five times that in HSCs or in KSL cells expressing the BCR-ABL mutant (Figure S5C). We also confirmed that these effects of BCR-ABL on KSL cells were reversed by imatinib treatment (Figures S5A–S5C). We further examined whether the difference in sensitivity to Fbxw7 deficiency between HSCs and LICs might be attributable to the difference in the abundance of c-Myc in these cells. Both exit from quiescence and apoptosis induced by *Fbxw7* deletion were more pronounced in HSCs overexpressing c-Myc and were less pronounced in $c\text{-}Myc^{+/\Delta}$ HSCs, than in control HSCs (Figures S5D and S5E). Accordingly, the decrease in the number of stem cells induced by Fbxw7 ablation in recipients of the second BMT was greater for HSCs overexpressing c-Myc, and smaller for $c\text{-}Myc^{+/\Delta}$ HSCs, than for control HSCs (Figure S5F).

We next compared sensitivity to combination therapy with

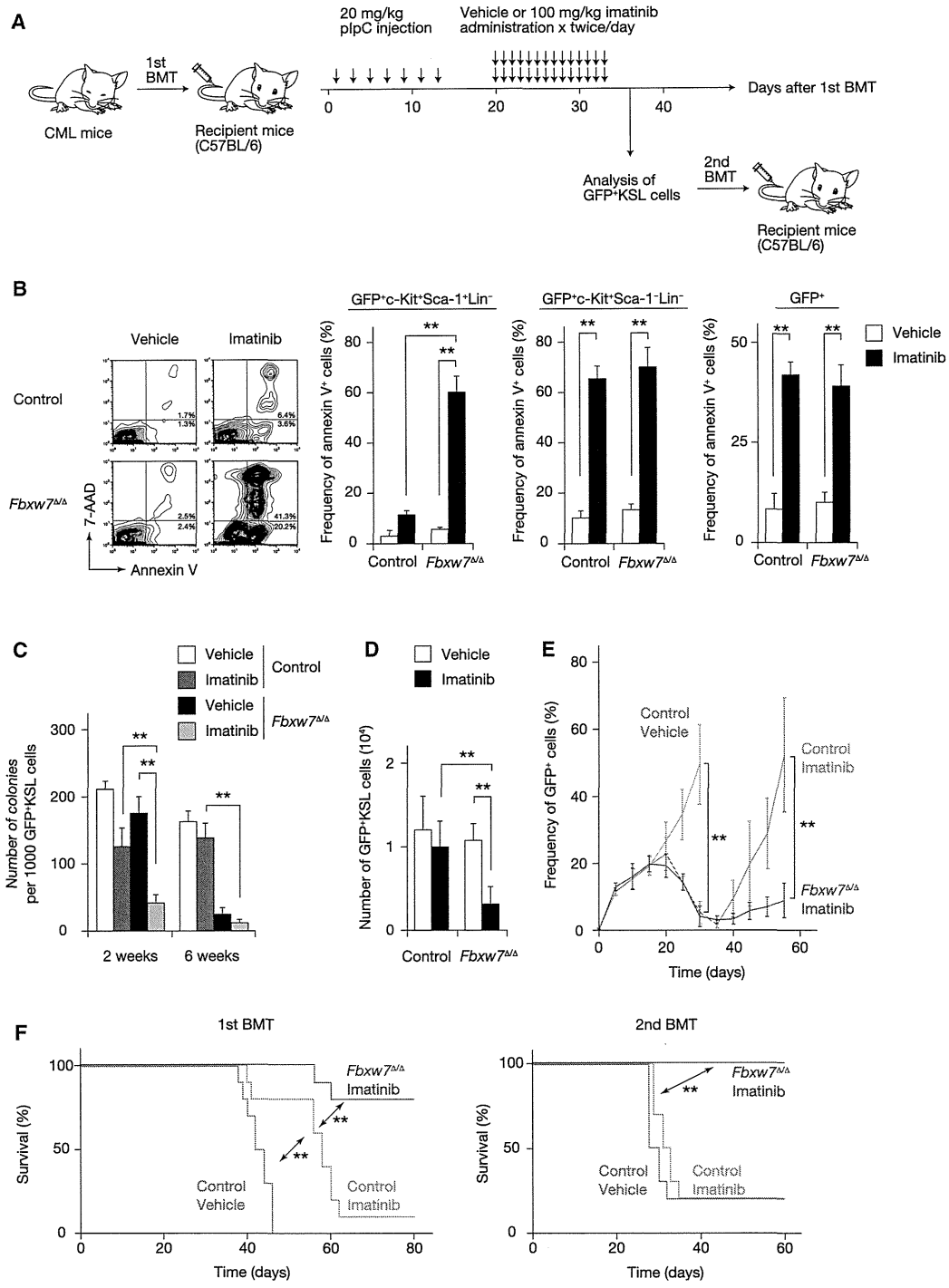

Figure 5. Combination Therapy with Fbxw7 Ablation and Imatinib Eliminates LICs

(A) Experimental strategy for combination therapy with Fbxw7 ablation and imatinib administration.

(B) Frequency of annexin V positivity among *Fbxw7*$^{\Delta/\Delta}$ or control cells of the indicated fractions isolated from recipients (n = 3) of the first BMT after treatment with imatinib or vehicle.

(C) Colony formation by *Fbxw7*$^{\Delta/\Delta}$ and control LICs cultured on OP-9 cells with imatinib or vehicle for 2 or 6 weeks (n = 3).

(D) Absolute number of GFP$^+$KSL cells in bone marrow from mice (n = 5) treated as in (A).

(E) Frequency of GFP$^+$ cells in peripheral blood from mice (n = 10) treated as in (A).

(F) Survival of recipients (n = 10) of the first and second BMT treated as in (A).

Data are means ± SD. **p < 0.01. See also Figure S4.

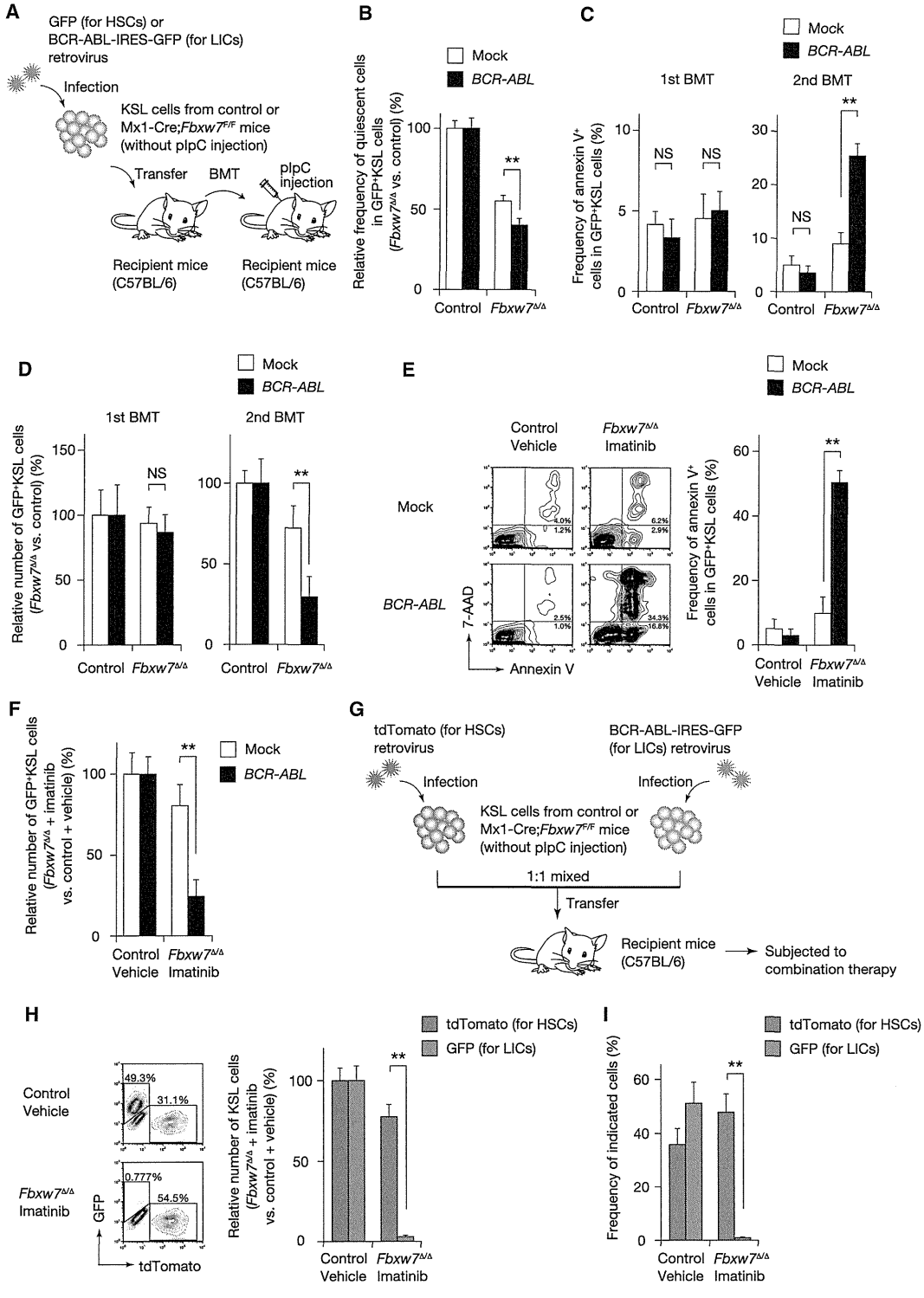

Figure 6. Fbxw7 Deficiency Affects LICs to a Greater Extent than It Does Normal HSCs

(A) Experimental strategy to compare the sensitivity of LICs to Fbxw7 deficiency with that of normal HSCs.

(B) The relative percentage of quiescent cells among GFP$^+$KSL cells for *Fbxw7*$^{\Delta/\Delta}$ cells compared with that for control cells infected with the corresponding vector was determined for recipients of the first BMT (n = 5).

(C) The frequency of annexin V$^+$ cells among GFP$^+$KSL cells for *Fbxw7*$^{\Delta/\Delta}$ cells compared with that for control cells infected with the corresponding vector was determined for recipients of the first and second BMTs (n = 3).

(legend continued on next page)